INFLUENCE OF DIAMOND BURNISHING PROCESS PARAMETERS ON STRAIN-INDUCED α'-MARTENSITE IN 304 CHROMIUM-NICKEL AUSTENITIC STAINLESS STEEL

Kalin Anastasov[1], Mariana Ichkova[1,2]

[1]Technical University of Gabrovo, 4 Hadji Dimitar St.
Gabrovo 5300, Bulgaria, kalinanastasov@tugab.bg (K.A.)
[2]Center of competence "Smart mechatronic, eco-and energy-saving systems and technologies", Technical University of Gabrovo
5300 Gabrovo, Bulgaria, ichkova@tugab.bg (M.I.)

Received 14 April 2025
Accepted 17 July 2025
DOI: 10.59957/jctm.v61.i1.2026.22

ABSTRACT

When chromium-nickel austenitic stainless steels must satisfy a requirement for a high degree of strain-hardening, the nickel content is limited to 8 - 9 wt. %. The surface cold working of these steels causes the martensitic transformation γ → α'. Thus, the surface microhardness and residual compressive stresses increase due to the presence of the harder strain-induced a'-martensite phase. This article investigates the influence of the governing factors of diamond burnishing (DB) on the percentage content of the a'-martensite in the surface layer of AISI 304 steel using planned experiment, analysis of variance and regression analysis. A mathematical model of the percentage content of a'-martensite depending on the burnishing force, feed rate and burnishing velocity was created. Of the three governing factors, the most significant is feed rate, and the least important is burnishing force. Thermal effects have a greater impact on martensitic transformation γ → α' compared to the mechanical effect. The percentage of martensite in the surface and subsurface layers is necessary information for determining the residual stresses by the X-ray method when studying the effect of DB on the surface integrity of austenitic stainless steels.

Keywords: austenitic stainless steel, strain-induced a'-martensite, surface plastic deformation, diamond burnishing.

INTRODUCTION

Chromium-nickel austenitic steels are widely used in many industries because of their superior general corrosion resistance, good machinability by cutting and plastic deformation, good weldability, and can be used in a wide temperature range: from cryogenic temperatures to 450°C; at higher temperatures there is a risk of intergranular corrosion [1]. A disadvantage of these steels under normal operating conditions is their insufficient hardness and strength. These properties can be improved by volume cold working or by surface layer (SL) modification [2, 3]. The former approach requires significant energy input and is limited to sheet metal blanks and parts. SL modification is achieved by low-temperature nitriding and/or carburizing to form the S-phase [4, 5], surface cold working [6, 7], or a combination of both [8, 9]. The formation of the S-phase is a valuable means of improving the hardness, fatigue strength, tribological properties and corrosion resistance of austenitic stainless steels. However, this process is time-consuming and expensive, due to its duration (typically 20 - 30 h) and the requirement of special and expensive equipment. In addition, the S-phase is a metastable phase due to its tendency to transform when exposed to high temperatures. The maximum operating temperature is about 200°C [4].

An effective approach to modify SL is surface cold working (SCW), which can be dynamic or static [10]. Dynamic methods such as shot peening and surface

mechanical attrition treatment are the successors of inventions by Tilgham sand blasting method [11] and are particularly effective for processing complex surfaces, but the resulting roughness is unsatisfactory [10].

In static SCW, a hard and smooth deforming element is pressed with a constant static force against the machined surface and performs relative movement with respect to it. In this way, the surface layer is plastically deformed at a temperature lower than the recrystallization temperature of the machined material. As a result, the roughness is drastically reduced, the surface microhardness is significantly increased, useful residual compressive stresses are introduced into the surface and nearby subsurface layers, and the microstructure in these layers is modified in the direction of grain refinement and orientation [12]. When the tangential contact between the deforming element and the machined surface is sliding friction, the static SCW is known as slide burnishing (SB) [13, 14]. SB is performed with a non-diamond [15, 16] or diamond [17] deforming element. In the latter case, SB is called diamond burnishing (DB). DB was introduced in 1962 by General Electric to improve the surface integrity (SI) of metal components. DB is a simple and effective finishing process and its main advantage over roller burnishing is the significantly simpler equipment with which DB is performed [18]. An experimental comparison between DB and deep rolling process [20] performed by Maximov et al. [19] showed the advantage of DB in terms of SI and fatigue strength characteristics.

Over the past six decades, DB has established itself as an effective finisher for structural [21], tool [22] and stainless [23, 24] steels, high-strength titanium [25] and aluminium [26, 27] alloys, and bronze alloys [28 - 30].

Extensive studies on the effects of the DB process on the SI and the fatigue, wear and corrosion resistance of specimens made of chromium-nickel austenitic steels have been conducted in [9, 12, 23, 31 - 35]. Since DB causes severe plastic deformation of the surface layers of these steels, part of the austenite in this layer and in the nearby subsurface layers is transformed into a'-martensite when the nickel content in the steel is below 15 wt. % [12, 23]. The austenite is stable when the nickel content is above 15 wt. %, because nickel reduces the ability of the austenite to strain hardening. When the chromium-nickel austenitic stainless steels must satisfy a requirement for a high degree of strain-hardening, the nickel content is limited to 8 - 9 wt. % [23]. DB causes the formation of two phases of strain-induced martensite: α' and e [23]. The second phase occurs because of smaller deformations. With increasing the degree of plastic deformation, the e-phase is transformed into α'-phase [36, 37].

As a harder phase, the α'-martensite increases the microhardness [23], but worsens the resistance to electrochemical corrosion [12]. The α' -martensite is metastable and after increasing the temperature the reverse transformation $\alpha' \rightarrow \gamma$ is observed. For example, Maximov et al. were shown that after heating at 450°C for two hours the DB-induced α'-martensite in the surface layer of 304 steel decreases almost by half [23]. It is difficult to assess which effect (the increased surface microhardness due to the induced α'-martensite or the introduced residual compressive stresses) has a dominant role in the increased fatigue strength of DBed specimens, due to the simple fact that both effects have a common physical basis: the equivalent plastic deformation of the surface layer [23]. However, the percentage content of martensite in the surface and subsurface layers is necessary information for determining the residual stresses by the X-ray method [31, 23], when studying the effect of DB on the SI of chromium-nickel austenitic stainless steels.

Thus, the main objective of this study is to determine the influence of the governing factors of the DB process on the strain-induced α'-martensite in the surface layer of DBed chromium-nickel austenitic stainless steel of the type 18/8.

EXPERIMENTAL

Material used

In this study, AISI 304 chromium-nickel austenitic stainless steel was chosen. This steel is of the 18/8 type and has excellent strain hardening ability. The material was obtained as hot-rolled bars with diameters of 16 mm and was used in as-received state. The chemical composition was established using optical emission spectrometer. Tensile tests at room temperature were carried out via Zwick/Roell Vibrophore 100 testing machine (Ulm, Germany). The working sections of the tensile test specimens have a gauge diameter of 6 mm and a gauge length of 30 mm. The material hardness was measured via a VEB-WPM tester (Germany) using

a spherical-ended indenter with a diameter of 2.5 mm, loading of 63 kg, and holding time of 10 sec.

DB implementation

DB (Fig. 1) was implemented on Index Traub CNC lathe using spherical-ended polycrystalline diamond insert with radius of 2 mm and conventional flood lubrication (Vasco 6000).

The burnishing devices (Fig. 1b) provide elastic normal contact between the deforming element and the treated surface. Turning as premachining and DB were carried out on CNC lathe in one clamping process to minimize the concentric run-out in DB. VCMT 160404-F3P carbide cutting insert (main back angle α_0 = 7°; radius at tool tip 0.4 mm) was used for the previous turning. SVJCR 2525M-16 holder with main and auxiliary setting angles χ_c = 93° and χ_c = 52°, respectively, was used. The cutting insert and the holder are manufactured by ISCAR Bulgaria.

Phase analysis and microstructure

To determine the percentage content of strain-induced martensite in the surface layer (relative to austenite), a Bruker D8 Advance diffractometer and (Billerica, MA, USA) a DIFFRAC.Dquant V1.5 specialized software developed by BRUKER company was used [51]. Crystallography Open Database was used to determine the peak positions. After polishing and etching with royal water, the microstructure in a cross-section area of the as-received bar was observed by means of optical microscopy (NEOPHOT 2, Carl Zeiss, Jena, Germany).

RESULTS AND DISCUSSION

Material identification

Table 1 shows the chemical composition of the used AISI 304 stainless steel. The remaining chemical elements (0.203 wt. %) are Ti, Al, Pb, Sn, Nb, B, As, Zn, Bi, Zr and Ca. The main mechanical characteristics in as-received state of the material are shown in Table 2.

Fig. 2 shows the diffraction pattern of the phase distribution of the used AISI 304 steel after turning. Three peaks of γ-ferrite (111), (200) and (220) are clearly observed. No broadening and displacement of the peaks are observed. The intensity of the three peaks coincides in relation to the intensity from the databases. The latter indicates that there are no texturing and

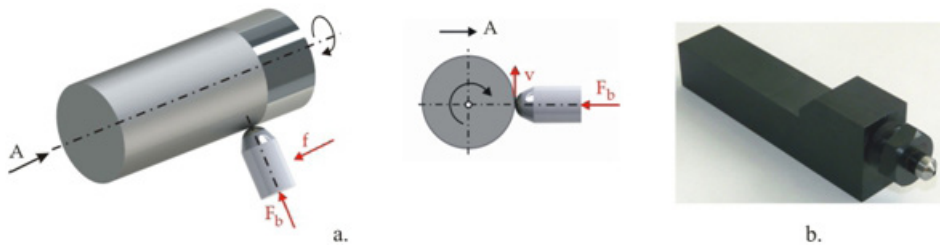

Fig. 1. DB implementation: (a) kinematics and governing factors; (b) DB device.

Table 1. Chemical composition (in wt. %) of the used AISI 304 stainless steel.

Fe	C	Si	Mn	P	S	Cr
69.51	0.023	0.271	1.600	0.047	0.034	19.19
Ni	Mo	Cu	Co	V	W	other
7.98	0.243	0.637	0.161	0.060	0.041	Balance

Table 2. Main mechanical characteristics of the tested AISI 304 stainless steel (as-received).

Yield limit, MPa	Tensile strength, MPa	Elongation, %	Hardness, HB
338^{+9}_{-18}	733^{+12}_{-10}	$44.7^{+0.3}_{-0.2}$	$250^{\pm 8}$

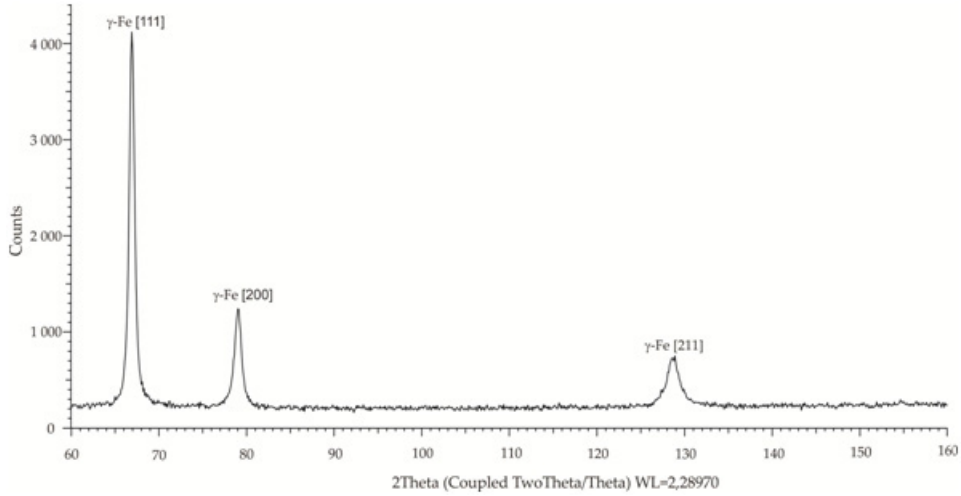

Fig. 2. Phase analysis results.

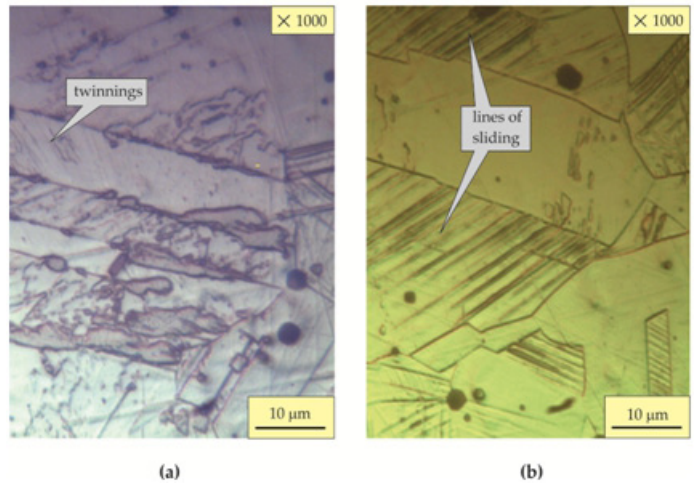

Fig. 3. Microstructure in as-received state: (a) near the surface layer; (b) in the core.

the presence of significant deformations in the steel structure. The presence of other phases is not observed. Fig. 3 shows the steel structure in the as-received state in two characteristic areas: near the surface (after turning) and in the core. In general, structural inhomogeneity is observed: zones with sliding stripes, zones with equiaxed austenite grains with an average size of 35 µm, twins and sliding zones within the grains themselves.

Experimental design

The governing factors were burnishing force F_b, feed rate f, and burnishing velocity v illustrated in Fig. 1a. The governing factor magnitudes (Table 3) were selected based on the results obtained by Maximov et al., where the authors have used one-factor-at-a-time method [23]. The radius of the spherical-ended diamond insert was maintained at a constant value of 2 mm; according to Maximov et al. this radius magnitude provides the highest microhardness [23]. The upper burnishing force level is 500 N, as higher values worsen the resulting roughness [23].

The transformation from physical (natural) $\tilde{x}_i$ to encoded (dimensionless) x_i variables is performed using the Eq. (1):

$$x_i = \frac{\left(\tilde{x}_i - \tilde{x}_{i,0}\right)}{\left(\tilde{x}_{i,max} - \tilde{x}_{i,0}\right)}, \quad (1)$$

where $\tilde{x}_{i,0}$ and $\tilde{x}_{i,max}$ are the average and maximum

Table 3. Governing factors and their levels.

Governing factors	Levels							
	Natural, $\tilde{x}_i$				Coded, x_i			
Burnishing force F_b, N	$\tilde{x}_1$	100	300	500	x_1	-1	0	1
Feed rate f [m/rev]	$\tilde{x}_2$	0.02	0.05	0.08	x_2	-1	0	1
Burnishing velocity v [m/min]	$\tilde{x}_3$	50	85	120	x_3	-1	0	1

Table 4. Experimental plan and results.

No	x_1	x_2	x_3	Srain-induced a'-martensite, %	
				Exper.	$Y_{\alpha'}$ model
1	-1	-1	-1	69.65	70.41
2	1	-1	-1	88.20	93.09
3	-1	1	-1	12.70	17.88
4	1	1	-1	63.60	60.00
5	-1	-1	1	49.60	53.20
6	1	-1	1	50.90	45.71
7	-1	1	1	07.50	2.61
8	1	1	1	15.30	14.54
9	-1	0	0	27.40	22.75
10	1	0	0	35.40	40.05
11	0	-1	0	76.00	71.92
12	0	1	0	26.00	30.07
13	0	0	-1	63.70	56.46
14	0	0	1	17.90	19.13

value of the physical variable, respectively.

The inverse transformation $x_i \rightarrow \tilde{x}_i$ is obtained from the Eq. (2):

$$\tilde{x}_i = \left(\tilde{x}_{i,max} - \tilde{x}_{i,0}\right)x_i + \tilde{x}_{i,0} . \quad (2)$$

The objective function was the percentage of strain-induced α'-martensite $Y_{\alpha'}$.

A planned experiment and a second-order optimal compositional design were used (Table 4).

The obtained experimental results are shown in Table 4. The average values of Ra roughness parameter and surface microhardness after turning and before DR were Ra^{init} = 0.529 μm and 421 HV, respectively.

Regression analysis was conducted using QStatLab software [39]. Given the chosen experimental design, the approximating polynomials are of the order no higher than the second (Eq. (3)):

$$Y_{\alpha'}(\{X\}) = b_0 + \sum_{i=1}^{3} b_i x_i + \sum_{i=1}^{2}\sum_{j=i-1}^{3} b_j x_i x_j + \sum_{i=1}^{3} b_i x_i^2 \quad (3)$$

where {X} is the vector of the governing factors x_i, i = 1, 2, 3.

The polynomial coefficients of the $Y_{\alpha'}$ model are shown in Table 5. The model-predicted percentage of srain-induced α'-martensite values at the experimental points are listed in Table 4. Except for experimental point 7, where the srain-induced α'-martensite is of no practical importance, the comparison with the experimental results shows good agreement between the model and the experiment.

From Eq. (3) and Table 5 for the function of induced martensite in dimensionless variables it follows the Eq. (4):

$$Y_{\alpha'} = 39.2594 + 8.655x_1 - 20.93x_2 - 15.66x_3 - 7.859x_1^2 + 11.74x_2^2 + 1.54x_3^2 + 4.8562x_1x_2 + 0.4812x_2x_3 - 7.544x_1x_3 \quad (4)$$

Statistical analysis of the regression models was performed using QStatlab. Critical value of the student statistics (T), Fisher statistics (F), residual standard deviation (ResStDev), determination coefficient (R-sq), and adjusted determination coefficient (Radj-sq) are as follows: T = 2.77645, F = 5.99878,

Table 5. Regression coefficients.

b_{ij}	b_0	b_1	b_2	b_3	b_{11}	b_{22}	b_{33}	b_{12}	b_{23}	b_{13}
$Y_{\alpha'}$	39.259	8.655	20.93	15.66	7.859	11.74	1.54	4.856	0.481	7.544

ResStDev = 8.8045, R-sq = 0.99542 and Radj-sq = 0.97933. The results, as well as the residuals in Table 4, confirm the model adequacy.

After substituting Eq. (1) into Eq. (4), for the function of induced martensite in physical variables, one obtains Eq. (5):

$$Y_{\alpha'} = 109.819 + 0.2123F_b - 2283.785f - 0.361v - - 0.0002F_b^2 + 13045.14f^2 + 0.00126v^2 + 0.8094F_bf + + 0.4583fv - 0.0011F_bv \quad (5)$$

The dimensionless absolute values of the coefficients b_i, i = 1, 2, 3 (Table 4) indicate the significance of the corresponding governing factor. The larger this value, the stronger the influence of the corresponding governing factor. The strongest influence on the strain-induced martensite is exerted by the feed rate $|b_2| = 20.93$. This is also confirmed by the absolute values of the coefficients b_{ij}, i = j: the coefficient b_2 has the largest absolute value. The explanation is that the feed directly affects the so-called cyclic loading coefficient (CLC), which is a measure of the amount of accumulated deformation in the surface layer, due to DB [40]. The larger the CLC, the greater the equivalent plastic deformation of the surface layer and hence the greater the percentage content of the induced martensite. A similar coefficient was also introduced by Kuznetsov et al. [41]. For the remaining two factors (burnishing force and burnishing velocity), it is difficult to judge which of them is more significant based on the method of comparing coefficients. The absolute value of b_3 is greater than that of b_1. Conversely, the absolute value of b_3 is smaller compared to that of b_1. To answer this question, analysis of variance (ANOVA) is required. The coefficients b_{ij}, $i \neq j$ provide information about the significance of the interactions between the factors. Obviously, the interaction between the burnishing force and burnishing velocity is the most significant ($|b_{13}| = 7.544$). The explanation is that the two factors act in the same direction: with an increase in each of them, the work from the friction forces and the work for plastic deformation increase. These works are transformed into a heat, which is the cause of the so-called softening effect [40, 42]. The more heat generated in the DB process, the more the content of induced martensite decreases. The weakest interaction is between the feed rate and burnishing velocity $|b_{23}| = 0.4812$. The interaction between burnishing force and feed rate occupies an intermediate position in importance. The two factors act unidirectionally with respect to the CLC, which considers the purely mechanical cause of surface deformation accumulation. Therefore, with respect to the induced martensite in DB process, the thermal effect dominates over the mechanical one in terms of interaction between the factors.

The ANOVA was conducted using QstatLab. The results obtained (Fig. 4) confirm that feed rate is the most significant factor, and burnishing force is the least significant. The latter confirms the conclusion made above, that the thermal effect dominates the mechanical one. α'- martensite is maximum. It is clearly seen that when the burnishing force is maintained at an upper level, and the other two factors (feed rate and burnishing velocity) occupy a lower level, the percentage content of the strain induced. The reason is that in this case

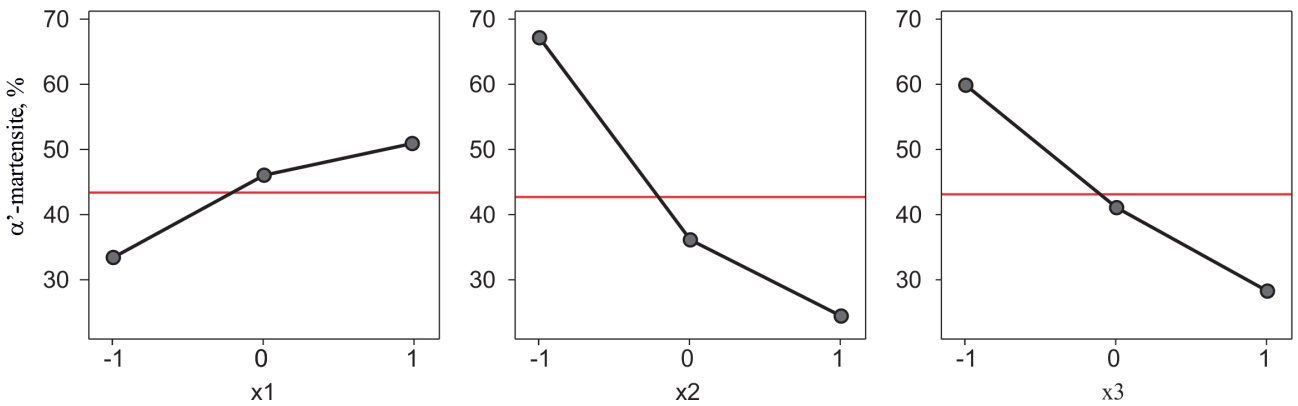

Fig. 4. ANOVA results: main effects of the strain-induced a'- martensite model.

the effect of the mechanical factor is maximum (the combination of maximum force and minimum feed rate maximizes the accumulated deformation), while the thermal effect is minimal due to the minimum value of burnishing velocity.

A graphical visualization of the strain-induced α'- martensite model is shown in Fig. 5. The visual inspection of the surfaces confirms the conclusions drawn about the significance of the governing factors and the interactions between them.

After substituting Eq. (1) into Eq. (3), the dependences of the strain-induced α'-martensite on the physical governing factors are obtained. Figs. 6, 7 and 8 show sections of the strain-induced α'-martensite hypersurface (the objective function) by means of characteristic hyperplanes. These sections visualize the dependence of the strain-induced α'-martensite on the corresponding governing factor and confirm the conclusions drawn above regarding the significance of the factors and their interactions.

With increasing the burnishing force, the strain-induced α'-martensite initially increases (Fig. 6), then shows a tendency to decrease, but at a different rate, depending on the combination of the magnitudes of the other two governing factors, which maintain constant values. As the burnishing force increases, the degree of plastic deformation increases, which leads to more induced martensite. At the same time, however, the greater force increases the power of friction forces, which increases the heat generated by friction and plastic deformation. As a result, the local temperature increases and hinders the martensitic transformation. In other words, the thermal effect of the burnishing force dominates over the mechanical effect caused by the same factor.

With increasing feed rate the strain-induced α'-martensite decreases, but at a noticeably decreasing rate (Fig. 7). The reason is the decreasing CLC defined

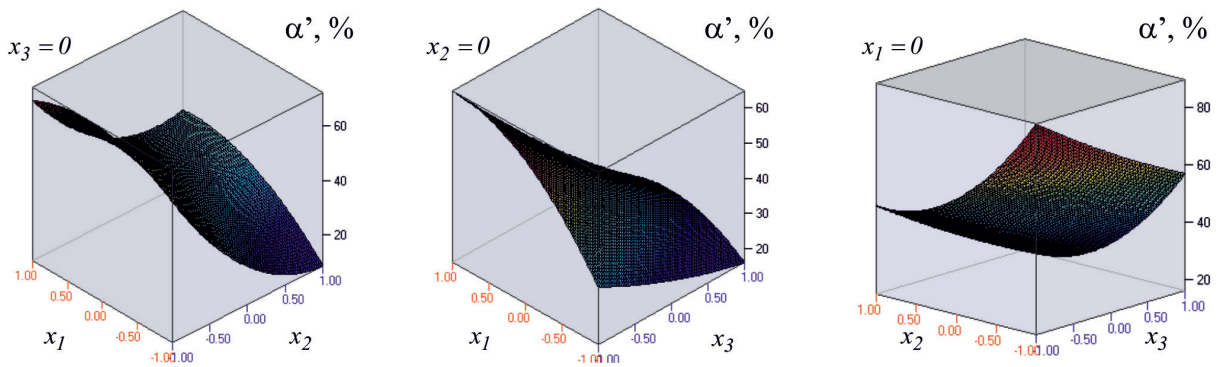

Fig. 5. Graphical visualization of the strain-induced α'- martensite model.

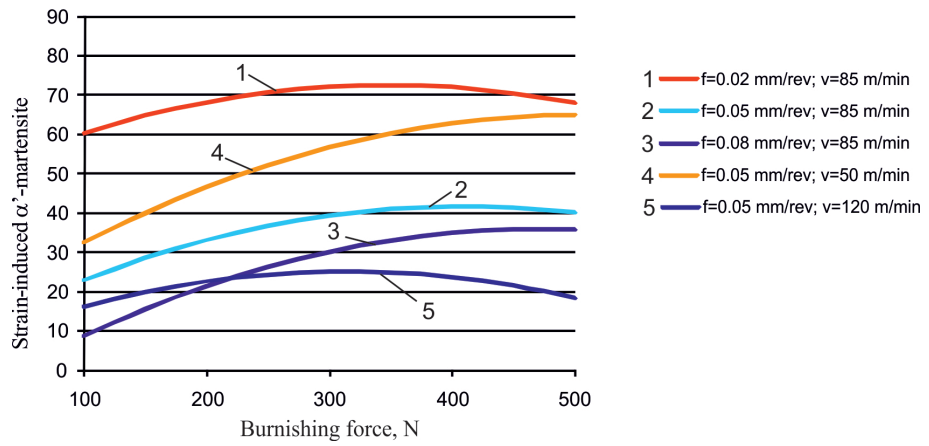

Fig. 6. Dependence of the strain-induced α'- martensite on the burnishing force.

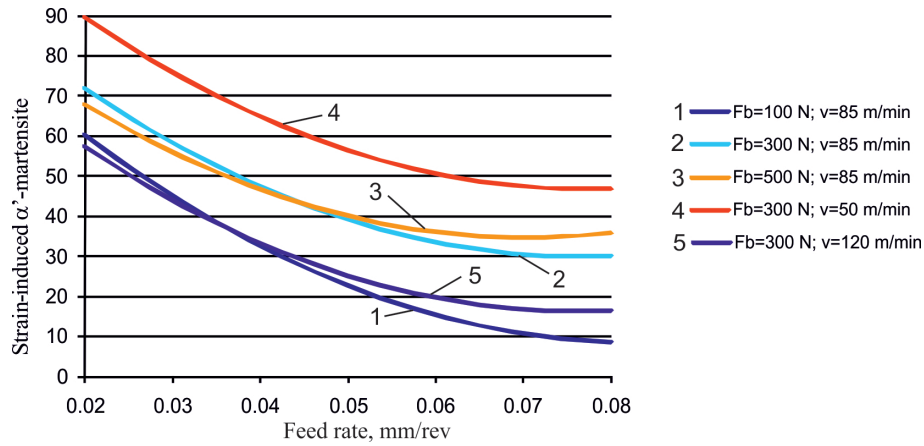

Fig. 7. Dependence of the strain-induced a'-martensite on the feed rate.

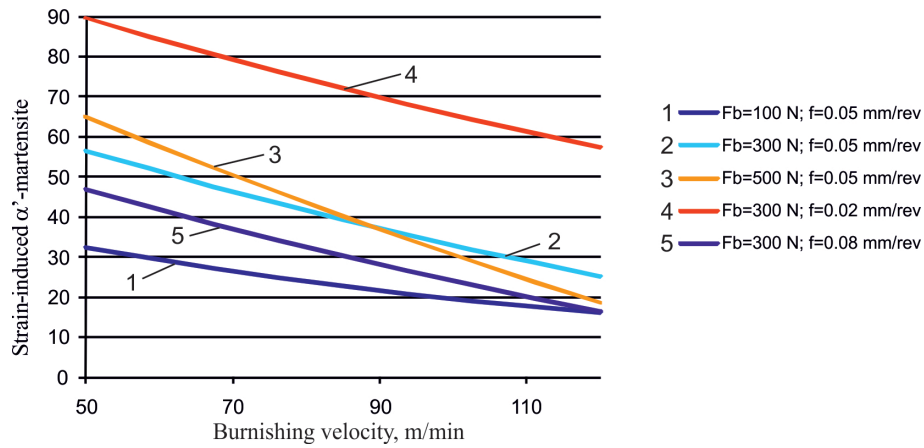

Fig. 8. Dependence of the strain-induced a'-martensite on the burnishing velocity.

in [40, 41]. On the other hand, increasing the feed rate reduces the local temperature in the vicinity of a point on the machined surface due to the decreasing CLC. This explains the slower rate of reduction of induced martensite when the feed rate increases.

With increasing the burnishing velocity, the strain-induced α'-martensite decreases (Fig. 8) approximately according to a linear law, in which the rate of reduction increases with increasing burnishing force. The linear law is determined by the fact that the heat flux density in the DB process depends linearly on the burnishing velocity. The higher burnishing velocity increases the power of the frictional forces, and thence the heat generated increases, suppressing the martensitic transformation $\gamma \rightarrow \alpha'$ [19]. At the same time, higher burnishing velocity leads to a higher rate of deformation. It is known that with increasing deformation rate, the material yield limit increases, approaching the tensile strength. In terms of DB, this means that the equivalent plastic deformation of the surface layer decreases, and thence the strain-induced α'-martensite decreases.

CONCLUSIONS

A comprehensive study of the effects of the governing factors of DB of AISI 304 steel specimens on the strain-induced α'-martensite in the surface layer was carried out using planned experiment, ANOVA and regression analysis. As a result, the major new findings (valid for the steel used and the ranges of variation of the governing factors) concerning the nature of DB process were:

- Mathematical model of the strain-induced α'-martensite depending on the burnishing force, feed rate and burnishing velocity was created.
- Of the three governing factors (burnishing force, feed rate and burnishing velocity), the most significant is feed rate, and the least important is burnishing force.
- The thermal effect has a greater weight for the martensitic transformation $\gamma \rightarrow \alpha'$ compared to the mechanical effect.
- With increasing the burnishing force, the strain-induced α'-martensite initially increases, then shows a tendency to decrease due to the increasing thermal effect.
- With increasing feed rate the strain-induced α'-martensite decreases, but with a noticeably decreasing speed, due to a reduction in the local temperature in the vicinity of a point on the treated surface.
- With increasing the burnishing velocity, the strain-induced α'-martensite decreases approximately linearly, with the rate of decrease increasing with increasing burnishing force.

Funding

This research was funded by the European Regional Development Fund under the Operational Program Scientific Research, Innovation and Digitization for Smart Transformation 2021-2027", Project CoC "Smart Mechatronics, Eco- and Energy Saving Systems and Technologies", BG16RFPR002-1.014-0005.

Authors' contributions

All authors contributed equally to the conception and design of the study. All authors have read and agreed to the published version of the manuscript.

REFERENCES

1. N.D. Rashkov, Heat treatment of steels, Sofia, Technika, 1977, (in Bulgarian).
2. A. Hedayati, A. Najafizadeh, A. Kermanpur, F. Forouzan, The effect of cold rolling regime on microstructure and mechanical properties of AISI 304L stainless steel, J. Mater. Process. Technol., 210, 2010, 1017-1022.
3. B.R. Kumar, A.K. Singh, S. Das, D.K. Bhattacharya, Cold rolling texture in AISI 304 stainless steel, Mater. Sci. Eng.A, 364, 2004, 132-139.
4. F. Borgioli, From austenitic stainless steel to expanded austenite - S phase: Formation, characteristics and properties of an elusive metastable phase, Metals, 20, 2020, 187.
5. Y. Hoshiyama, R. Mizobata, H. Miyake, Mechanical properties of austenitic stainless steel treated by active screen plasma nitriding, Surf. Coat. Technol., 307, 2016, 1041-1044.
6. P. Juijerm, I. Altenberger, Fatigue performance enhancement of steels using mechanical surface treatments, J. Met. Mater. Miner., 17, 1, 2007, 59-65.
7. P. Juijerm, I. Altenberger, Fatigue performance of high-temperature deep-rolled metallic materials, J. Met. Mater. Miner., 17, 2, 2007, 37-41.
8. Y. Lin, J. Lu, L. Wang, T. Xu, Q. Xue, Surface nanocrystalization by surface mechanical attrition treatment and its effect on structure and properties of plasma nitrided AISI 321 stainless steel, Acta Mater., 54, 2006, 5599-5605.
9. J.T. Maximov, G.V. Duncheva, A.P. Anchev, V.P. Dunchev, Y.B. Argirov, Improvement in fatigue strength of chromium-nickel austenitic stainless steels via diamond burnishing and subsequent low-temperature gas nitriding, Applied Sciences, 2024, 14, 1020.
10. G. Duncheva, J. Maximov, Cold working technologies for increasing the fatigue life of metal structural components with fastener holes - review and perspectives, Int. J. Adv Manuf. Technol., 136, 2025, 2909-2943
11. H.J. Plaster, A tribute to Benjamin chew Tilghman, in: proceedings of the 5th international conference on shot peening, 1993, 2-9.
12. J.T. Maximov, G.V. Duncheva, A.P. Anchev, V.P. Dunchev, Y.B. Argirov, M.P. Nikolova, Effects of heat treatment and diamond burnishing on fatigue behaviour and corrosion resistance of AISI 304 austenitic stainless steel. Applied Sciences, 13, 2023, 2570.
13. M. Korzynski, Slide diamond burnishing. in: Nonconventional Finishing Technologies, Ed. M. Korzynski, Polish Scientific Publishers PWN, Warsaw, 2013, 9-33.
14. H. Roohi, H. Baseri, M. Mirnia, Evaluation of

optimized surface characteristics in non-rotational sliding ball burnishing, Mater. Manuf. Proces., 39, 16, 2024, 2299-2308.
15. J.T. Maximov, G.V. Duncheva, Finite Element Analysis and optimization of spherical motion burnishing of low-alloy steel, Proc IMechE, Part C: J. Mech. Eng. Sci., 226, 1, 2012, 161-176.
16. J.T. Maximov, T.V. Kuzmanov, G.V. Duncheva, N. Ganev, Spherical motion burnishing implemented on lathes, Int. J. Mach. Tools. Manuf., 49, 11, 2009, 824-831.
17. H. Luo, J. Liu, Q. Zhong, Investigation of the burnishing process with PCD tool on non-ferrous metals, Int. J. Adv. Manuf. Technol., 25, 5-6, 2005, 454-459.
18. G.V. Duncheva, J.T. Maximov, V.P. Dunchev et al. Single toroidal roller burnishing of 2024-T3 Al alloy implemented as mixed burnishing process, Int. J. Adv. Manuf. Technol., 111, 2020, 3559-3570.
19. J.T. Maximov, G.V. Duncheva, A.P. Anchev, V.P. Dunchev, Slide burnishing versus deep rolling - a comparative analysis, J. Adv. Manuf. Technol., 110, 2020, 1923-1939.
20. I. Nikitin, I. Altenberger, Comparison of the fatigue behavior and residual stress stability of laser-shock peened and deep rolled austenitic stainless steel AISI 304 in the temperature range 25-600^{o}C, Mater. Sci. Eng. A, 465, 2007, 176-182.
21. J.T. Maximov, G.V. Duncheva, A.P. Anchev, V.P. Dunchev, Smoothing, deep or mixed diamond burnishing of low-alloy steel components – optimization procedures, J. Adv. Manuf. Technol., 106, 2020, 1917-1929.
22. D. Tobola, B. Kania, Phase composition and stress state in the surface layers of burnished and gas nitrided Sverker 21 and Vanadis 6 tool steels, Surf. Coat. Technol., 353, 2018, 105-115.
23. J.T. Maximov, G.V. Duncheva, A.P. Anchev, V.P. Dunchev, Y.B. Argirov, Effect of diamond burnishing on fatigue behaviour of AISI 304 chromium-nickel austenitic stainless steel, Materials, 15, 14, 2022, 4768.
24. M. Korzynski, K. Dudek, B. Kruczek, P. Kocurek, Equilibrium surface texture of valve stems and burnishing method to obtain it, Tribol. Int., 124, 2018, 195-199.
25. D. Toboła, J. Morgiel, L. Maj, TEM analysis of surface layer of Ti-6Al-4V ELI alloy after slide burnishing and low-temperature gas nitriding, Appl. Surf. Sci., 515, 2020, 145942.
26. J.T. Maximov, A.P. Anchev, G.V. Duncheva, N. Ganev, K.F. Selimov, V.P. Dunchev, Impact of slide diamond burnishing additional parameters on fatigue behaviour of 2024-T3 Al alloy, Fatigue Fract. Eng. Mater. Struct., 42, 1, 2019, 363-373.
27. J.T. Maximov, A.P. Anchev, V.P. Dunchev et al., Effect of slide burnishing basic parameters on fatigue performance of 2024-T3 high-strength aluminium alloy, Fatigue Fract. Eng. Mater. Struct., 40, 11, 2017, 1893-1904.
28. G.V. Duncheva, J.T. Maximov, N. Ganev, G.V. Duncheva, K.F. Selimov, Enhancement of the wear resistance of CuAl9Fe4 sliding bearing bushings via diamond burnishing, Wear, 510-511, 2022, 204491.
29. G.V. Duncheva, J.T. Maximov, A.P. Anchev, V.P. Dunchev, Y.B. Argirov, Multi-objective optimization of internal diamond burnishing process, Mater. Manuf. Process., 37, 4, 2022, 428-436.
30. G.V. Duncheva, J.T. Maximov, A.P. Anchev, V.P. Dunchev, Y.B. Argirov, Improvement in wear resistance performance of CuAl8Fe3 single-phase aluminum bronze via diamond burnishing, J. Mater. Eng. Perform., 31, 2022, 2466-2478.
31. J.T. Maximov, G.V. Duncheva, A.P. Anchev, V.P. Dunchev, Explicit correlation between surface integrity and fatigue limit of surface cold worked chromium-nickel austenitic stainless steels, Int. J. Adv. Manuf. Technol., 133, 2024, 6041-6058.
32. G. Varga, V. Ferencsik, Experimental examination of surface micro-hardness improvement ratio in burnishing of external cylindrical workpieces, Cutting and Tools in Technological System, 93, 2020, 114-121.
33. M. Okada, M. Shinya, H. Matsubara, H. Kozuka, H. Tachiya, N. Asakawa, M. Otsu, Development and characterization of diamond tip burnishing with a rotary tool, J. Mater. Process. Technol., 244, 2017, 106-115.
34. J. Maximov, G. Duncheva, A. Anchev, V. Dunchev, K. Anastasov, Y. Argirov, Sustainable Diamond Burnishing of Chromium-Nickel Austenitic Stainless Steels: Effects on Surface Integrity and Fatigue Limit, Appl. Sci., 14, 2024, 9031.
35. A. Skoczylas, K. Zaleski, J. Matuszal, K. Ciecieląg, R. Zaleski, M. Gorgol, Influence of slide burnishing

parameters on the surface layer properties of stainless steel and mean positron lifetime, Materials, 15, 2022, 8131.
36. P.L. Mangonon, G. Thomas, The martensite phases in 304 stainless steel, Metall. Trans., 1, 1970, 1577-1586.
37. P.L. Mangonon, G. Thomas, Structure and properties of thermal-mechanically treated 304 stainless steel, Met. Mater. Trans. A, 1, 1970, 1587-1594.
38. Diffrac. DQUANT, Quantitative Analysis from Calibration to Reporting; Bruker AXS GmbH, Karlsrue, Germany, 2018.
39. I.N. Vuchkov, I.I. Vuchkov, QStatLab Professional, version 6.1.1.3, Statistical Quality Control Software, User's Manual, QStatLab, Sofia, Bulgaria, 2009.
40. J.T. Maximov, G.V. Duncheva, A.P. Anchev, N. Ganev, V.P. Dunchev, Effect of cyclic hardening on fatigue performance of slide burnishing components made of low-alloy medium carbon steel, Fatigue Fract.Eng.Mater.Struct., 42, 6, 2019, 1414-1425.
41. V.P. Kuznetsov, I.Y. Smolin, A.I. Dmitriev, S.Y. Tarasov, V.G. Gorgots, Toward control of subsurface strain accumulation in nanostructuring burnishing on thermostrengthened steel, Surf. Coat. Techol., 285, 2016, 171-178.
42. J.T. Maximov, G.V. Duncheva, A.P. Anchev, N. Ganev, I.M. Amudjev, Effect of slide burnishing method on the surface integrity of AISI 316Ti chromium-nickel steel, J. Braz. Soc. Mech. Sci. Eng., 2018, 40, 194.